Design and Characterization of Stormram 4: An MRI-Compatible Robotic System for Breast Biopsy

Vincent Groenhuis[1], Françoise J. Siepel[1], Jeroen Veltman[2] and Stefano Stramigioli[1]

***Abstract*— Targeting of small lesions with high precision is essential in an early phase of breast cancer for diagnosis and accurate follow up, and subsequently determines prognosis. Current techniques to diagnose breast cancer are suboptimal, and there is a need for a small, MRI-compatible robotic system able to target lesions with high precision and direct feedback of MRI. Therefore, the design and working mechanism of the new Stormram 4, an MRI-compatible needle manipulator with four degrees of freedom, will be presented to take biopsies of small lesions in the MRI scanner. Its dimensions (excluding racks and needle) are 72x51x40 mm, and the system is driven by two linear and two curved pneumatic stepper motors. The T-26 linear motor measures 26x21x16 mm, has a nominal step size of 0.25 mm and the measured maximum force is 63 N at 0.65 MPa. The workspace has a total volume of 2.2 L.**

Accuracy measurements have shown that the mean positioning error is 0.7 mm, with a reproducibility of 0.1 mm. Velocity measurements with 5 m long tubes show a maximum stepping frequency of 8 Hz (maximum force) to 30 Hz (unloaded). These results show that the robot might be able to target lesions with sub-millimeter accuracy within reasonable time for the MRI-guided breast biopsy procedure.

I. INTRODUCTION

A. Clinical challenge

Breast cancer is one of the most frequently diagnosed cancer types with an estimated 1.67 million new cancer cases in 2012, and the leading cause of cancer-related death among women worldwide [1]. In breast cancer screening, suspicious lesions need to be biopsied for pathological confirmation of the diagnosis. Some abnormalities are occult on mammography and ultrasound and can only be detected with MRI. In these cases a biopsy will be taken of the, often small, suspicious lesion under MRI-guidance. In current clinical practice, the needle must be inserted manually with the patient moved in and out of the scanner-bore multiple times for position adjustment and verification [2], [3].

This phase of the biopsy procedure is time-consuming and because of deformations due to needle-tissue interactions and patient movements, the needle may need to be re-positioned by using an alternate trajectory or multiple insertions leading to additional tissue damage and inaccurate placement [4].

Increased needle positioning accuracy and efficiency using a robotic system could improve the standard of care for women with a MRI detected lesion. If such a system is able to insert the needle inside the MRI scanner and is MRI-compatible itself, (near-)realtime imaging feedback is possible and enhances accuracy. Therefore, the aim of this project was to design and characterize an MRI-compatible robotic system for breast biopsy.

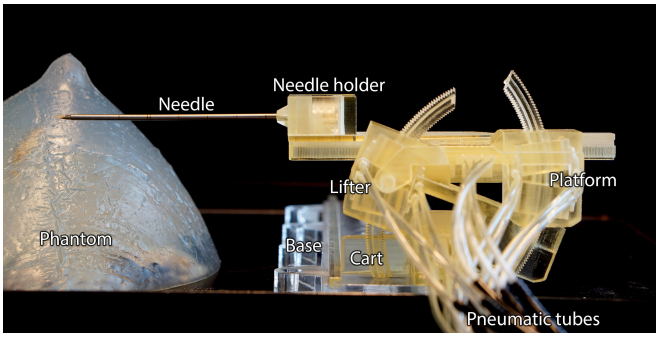

Fig. 1: The Stormram 4 robot.

B. State-of-art

Previous studies showed the design of robotic systems in several applications inside the MRI scanner. Stoianovici et al. developed the MrBot [5], a six DOF robotic system for prostate biopsy and driven by pneumatic rotational stepper motors. These motors have good specifications, but are also relative and complex to build. Bomers et al. developed a five DOF robot for prostate biopsy guidance [8], driven by pneumatic screw-motion stepper motors which, while useful in this application, are difficult to use in smaller scale robotics. Franco et al. developed a four DOF robot for liver biopsy, driven by relatively large pneumatic cylinders with a time-delay control scheme [6], which is difficult to control precisely due to the complex pneumatic model. Hungr et al. developed a five DOF robotic system for liver biopsy [7]. This system is driven by a combination of ultrasonic motors, Bowden cables and pneumatic actuators, making it also relatively complicated to develop.

The authors of the current paper, Groenhuis et al., developed three robotic systems for breast biopsy. The Stormram 1 is a seven DOF needle manipulator driven by 72 mm-sized pneumatic linear stepper motors [9] with a force of 24 N. For the Stormram 2, the motors were miniaturized to fit inside 45 mm-sized ball joints [10] and driven by a computerized valve manifold [11]. The Stormram 3 has five degrees of freedom, improved accuracy and workspace, and utilizes the T-49 stepper motor which can exert 100 N so that more dense tissue can be targeted.

[1]Vincent Groenhuis, Françoise J. Siepel and Stefano Stramigioli are with Robotics and Mechatronics, Faculty of Electrical Engineering, Mathematics and Computer Science, University of Twente, Enschede, The Netherlands. E-mail: v.groenhuis@utwente.nl, f.j.siepel@utwente.nl, s.stramigioli@utwente.nl

[2]Jeroen Veltman is with Ziekenhuisgroep Twente, Almelo, The Netherlands. E-mail: j.veltman@zgt.nl

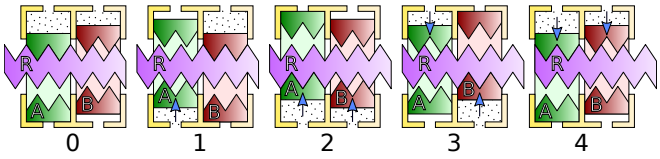

Fig. 2: Sequence of states in two-cylinder linear motor. The pistons are labeled A and B, the rack is labeled R. The arrows indicate piston movements, causing step-wise movement of the rack to the right.

The described robots are all parallel manipulators. While such a kinematic chain increases structural rigidity, it also limits the workspace and makes forward/inverse kinematics relatively complicated. The Stormram 3 also cannot move the needle along a straight path.

C. Approach

Our approach is to use a serial kinematic chain, driven by a combination of linear and novel curved pneumatic stepper motors. If rigidity can be preserved under the absence of metallic materials, a serial kinematic chain offers important advantages in terms of structural/kinematic complexity, controllability and workspace size. The robot can be made inherently MRI safe by the choice of materials and using pneumatic actuation.

II. DESIGN AND IMPLEMENTATION

A. Robot design

The presented Stormram 4 robot is a needle manipulator with four degrees of freedom placed in a serial kinematic chain. The four joints are actuated by pneumatic stepper motors. In its home position (Fig. 11), the robot (excluding needle and racks) measures 72 mm × 51 mm × 40 mm.

Fig. 1 shows the different parts of the robot. The base is fixed and has a rack, on which the cart can slide back and forth over a distance of 160 mm. The cart itself contains a curved rack, which the lifter uses to tilt itself upwards over an angle up to 47°. Likewise, the lifter has another curved rack on which the platform can tilt to the other side over an angle up to 38°. Finally, the platform drives a needle holder back and forth over a distance of 80 mm, on which the needle itself is mounted to target a breast phantom. The phantom is placed on a simple platform next to the robot. Not included is the option of horizontal angulation, in order to make the robot as compact as possible. Sixteen pneumatic tubes guide air to the different chambers of the four motors. The mass of the Stormram 4 (without base) is 62 g.

B. Stepper motors

Two different stepper motors have been developed for the Stormram 4: the T-26 linear motor, and the C-30 curved motor. The general mechanism is shown in Fig. 2. It shows a rack (purple) and two double-acting pistons (red, green). Each piston consists of two piston heads, with jaws on the inside that engage on the rack by means of a wedge mechanism. By pressurizing the four chambers with appropriate waveforms, the pistons push the rack step by step in the desired direction.

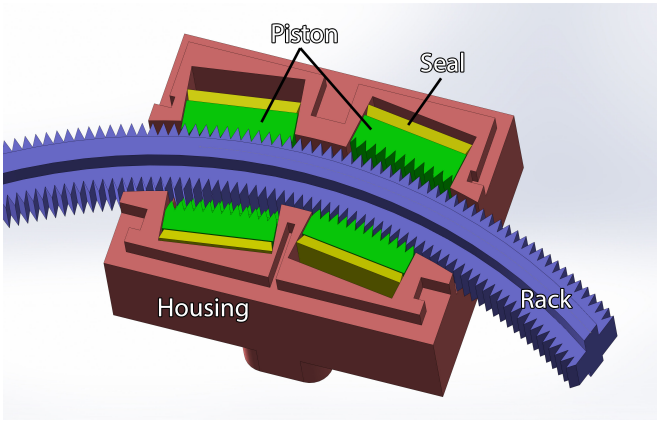

Fig. 3: C-30 curved stepper motor with opened housing, exposing the rack, pistons and seals.

By design, the motor has zero backlash and nonzero hysteresis. The reason is that both pistons simultaneously push on the rack, but only one can be at its extreme position as can be seen in Fig. 2. The piston which is not at the extreme position, therefore acts as a wedge between the rack's teeth and the cylinder wall, which fixates the rack in its position resulting in zero backlash.

1) Linear stepper motor: The T-26 linear stepper motor is a miniaturization of the T-49 motor described in [12]. The T-26 measures 26 mm × 21 mm × 16 mm. The two cylinders inside this motor have a square cross-sectional area of 10 mm × 10 mm = 100 mm^2. The pistons act on a straight rack with teeth pitch 1.0 mm and teeth depth 1.2 mm. The step size is 0.25 mm, which is one-quarter of the pitch. The wedge ratio is $\frac{1.2}{0.5} = 2.4$, so at a pressure of 0.4 MPa the theoretical output force is $F = 0.4 \cdot 10^6 \cdot 100 \cdot 10^{-6} \cdot 2.4 = 96\,\mathrm{N}$, or $240\,\mathrm{N/MPa}$. Due to friction in the seals and other sliding parts, the measured output force will be lower. If desired, the pressure can be increased to compensate for it and generate higher forces.

2) Curved stepper motor: The C-30 curved stepper motor is a novel design and measures 30 mm × 23 mm × 14 mm (excluding tube sockets). A 3-D rendering of the C-30 (without top cover) is shown in Fig. 3. The C-30 also houses two cylinders with the same square cross-sectional area of 100 mm^2 as in the T-26 linear stepper motor. The difference is that the rack is not straight, but has a radius of curvature of 50 mm. The teeth pitch size is 1.0°, which corresponds to an effective pitch distance of 0.87 mm on a circle with radius 50 mm. The step size is 0.25°, which is one quarter of the pitch size. The teeth depth is 1.2 mm. At a pressure of 0.2 MPa, the theoretical output torque is $M = 0.2 \cdot 10^6 \cdot 100 \cdot 10^{-6} \cdot 1.2 \cdot 10^{-3} \cdot \frac{180}{0.5\pi} = 1.38\,\mathrm{N\,m}$, or 55 N at an arm length of 50 mm. Similar to the T-26 motor, the measured output force will be lower due to friction in the seals and other sliding parts, which can be compensated for by increasing the pressure.

Fig. 4: Computerized manifold.

The curved stepper motor has an axis of rotation. Therefore, a physical joint driven by this actuator can be combined with a passive pin joint with small radius, placed at the axis of rotation. This is useful to significantly increase the rigidity of the joint. In the linear stepper motor this would not be an option, as its axis of rotation is located at infinity.

C. Production

The parts of the Stormram 4 were printed with the Stratasys Objet Eden260 (Stratasys Ltd., Eden Prairie, MN, USA) in FullCure720 material. The seals were laser-cut from 0.5 mm thick silicone rubber. The motor housing and cover were glued together, and the sixteen polyurethane tubes were also glued into the sockets. The base was laser-cut from an 8 mm plate, engraved with grooves in which the linear rack and guide rail were glued.

D. Controller

The robot is controlled by a pneumatic valve manifold, shown in Fig. 4. The pneumatic routing for two valves connected to one motor is shown in Fig. 5. The eight valves are of type Festo MHA2-MS1H-5/2-2, and are controlled with an Arduino Mega board. Two different tube lengths were tested: 0.5 m and 5 m.

A user interface allows to control the robot in different ways. The stepping frequency is controlled by one turn knob. In manual control mode, four other turn knobs reflect the setpoints of the four joints to which the robot is steered. In automatic mode, the controller steers the robot through a pre-programmed sequence of setpoints instead.

The display shows the joint configuration vector or the needle tip position and orientation. Pushbuttons allow to cycle through different information panels and enable various actions such as calibration or automatic mode initiation. Voltage and pressure sensors examine operational status. Upon loss of pressure or voltage, the valves are switched off and the current joint coordinates are stored in memory.

III. KINEMATICS AND WORKSPACE

Fig. 6 shows a sequence of states during the needle alignment and insertion process. It shows the effect of actuation of three different joints, allowing to align and insert the needle in the YZ-plane towards a given location.

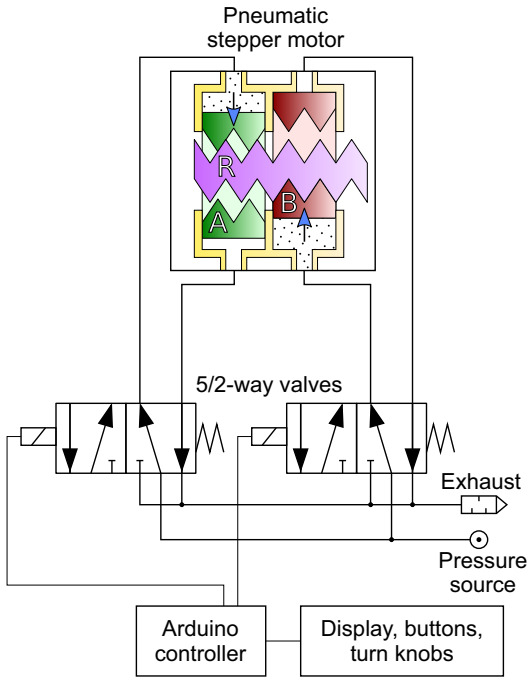

Fig. 5: Pneumatic routing for one stepper motor. Two 5/2-way valves are connected to one motor, to pressurize the right chambers according to signals from the Arduino controller.

Fig. 7 shows the kinematic configuration of the Stormram 4. Kinematically, it is a serial manipulator with four actuated joints. $J1$ and $J4$ are prismatic joints, driven by linear stepper motors. Joints $J2$ and $J3$ are rotational joints, driven by curved stepper motors. Point E is the end-effector, physically the tip of the needle. Its coordinates are (E_x, E_y, E_z, ϕ), in which ϕ is the rotation angle around the X-axis, with $\phi = 0°$ being horizontal.

The joint configuration vector $\mathbf{v} = (\ell_1, \alpha, \beta, \ell_4)$ defines the pose of the full robot. The range of these variables are:

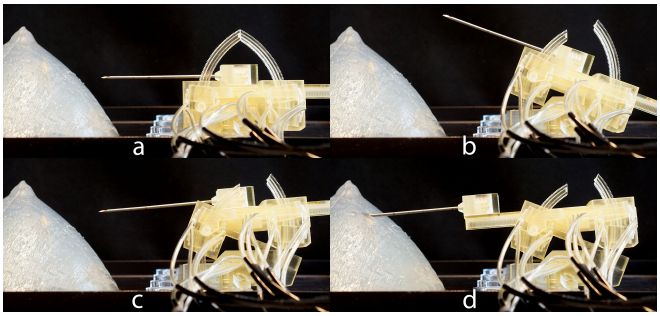

Fig. 6: Four consecutive states in the needle alignment and insertion sequence.

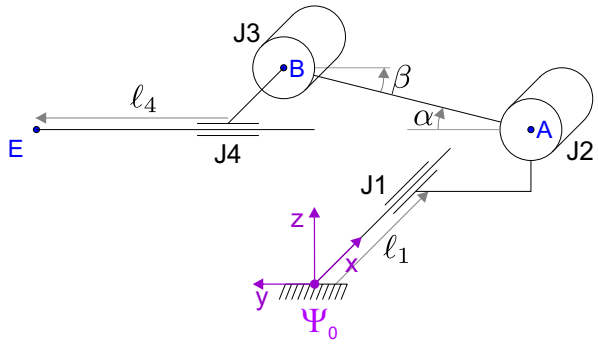

Fig. 7: Kinematic configuration.

$$
\begin{aligned}
\ell_1 &: 0\,\text{mm}..160\,\text{mm} \\
\alpha &: 0°..47° \\
\beta &: 0°..38° \\
\ell_4 &: 65\,\text{mm}..145\,\text{mm}
\end{aligned}
$$

The step size of ℓ_1 and ℓ_4 is 0.25 mm, and the step size of α and β is 0.25°.

In order to translate $\mathbf{v}$ to position and orientation of E and vice-versa, forward and inverse kinematics are derived.

A. Forward kinematics

The end-effector coordinates are calculated as follows:

$$
\begin{aligned}
E_x &= \ell_1 \\
E_y &= Y_0 + W_1 \cos\alpha - H_2 \sin(\alpha - \beta) + \ell_4 \cos(\alpha - \beta) \\
E_z &= H_1 + W_1 \sin\alpha + H_2 \cos(\alpha - \beta) + \ell_4 \sin(\alpha - \beta) \\
\phi &= \alpha - \beta
\end{aligned}
$$

The constants are:

$$Y_0 = -61\,\text{mm}, H_1 = 15\,\text{mm}, W_1 = 50\,\text{mm}, H_2 = 18\,\text{mm}$$

B. Inverse kinematics

Given the desired end-effector location and orientation (E_x, E_y, E_z, ϕ), the joint vector $\mathbf{v} = (\ell_1, \alpha, \beta, \ell_4)$ was calculated. Geometrically, this is equivalent to one particular intersection of a line with a circle in the YZ-plane. We first transformed (E_y, E_z) to (E'_y, E'_z), and then found an expression involving ℓ_4:

$$
\begin{aligned}
E'_y &= E_y + H_2 \sin\phi - Y_0 \\
E'_z &= E_z - H_2 \cos\phi - H_1 \\
W_1^2 &= (E'_y - \ell_4 \cos\phi)^2 + (E'_z - \ell_4 \sin\phi)^2
\end{aligned}
$$

Solving for ℓ_4 and taking the solution with smallest value, leads to:

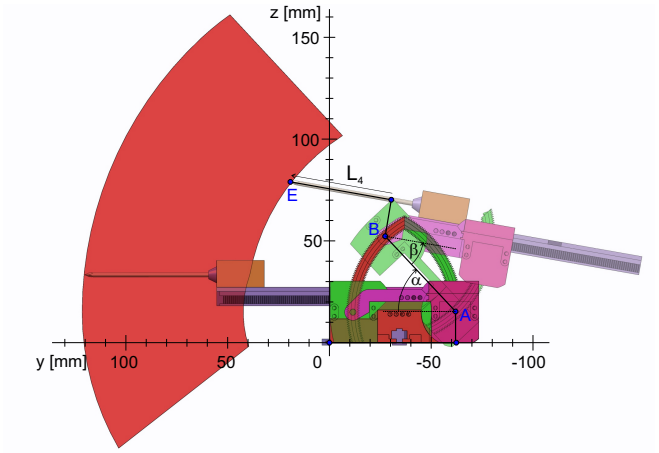

Fig. 8: Workspace, and two extreme poses of the Stormram 4.

$$
\begin{aligned}
\ell_1 &= E_x \\
\ell_4 &= E'_y \cos\phi + E'_z \sin\phi \\
&\quad - \sqrt{(E'_y \cos\phi + E'_z \sin\phi)^2 - E'^2_y - E'^2_z + W_1^2} \\
\alpha &= \arcsin \frac{E'_z - \ell_4 \sin\phi}{W_1} \\
\beta &= \alpha - \phi
\end{aligned}
$$

The solution is valid if ℓ_4 is real, and all parameters $(\ell_1, \alpha, \beta, \ell_4)$ are within the ranges.

Due to discretization of the stepper motors, the actual value of the four parameters must be a multiple of its step size (0.25 mm or 0.25°). The general approach is to round each parameter to its nearest reachable value, leading to end-effector positioning errors of the same order as the step size. This error could be reduced if the angle ϕ can be chosen: the optimal angle ϕ is the one (within its allowed range) which minimizes the end-effector positioning error.

C. Workspace

Fig. 8 shows the projection of the robot on the YZ plane in two different poses. One pose has configuration vector $\mathbf{v} = (0\,\text{mm}, 47°, 38°, 65\,\text{mm})$. The red area is the projected reachable space of the end-effector E, and its area is calculated to be 140 cm^2. The robot can move in the X-direction over a distance of 160 mm orthogonal to the YZ plane, resulting in a total workspace volume of 2.2 L.

IV. MEASUREMENTS AND RESULTS

Performance measurements of the stepper motors and measurements on Stormram 4's positional accuracy have been performed to characterize the Stormram 4.

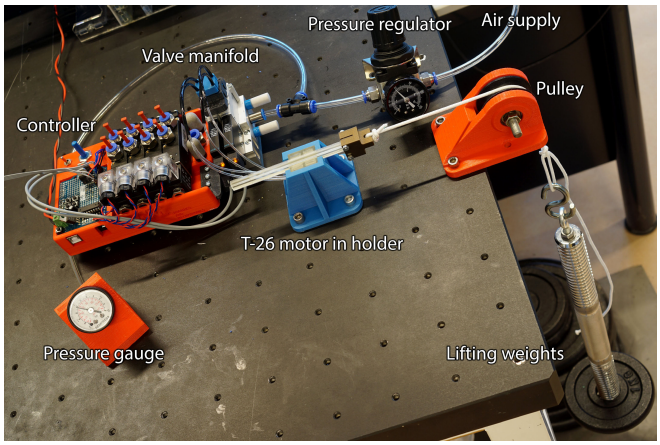

Fig. 9: T-26 force measurement setup.

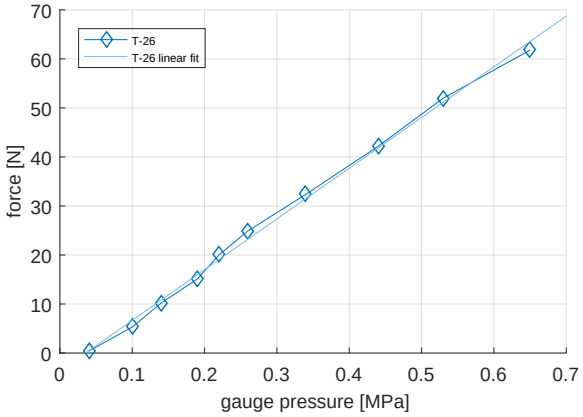

Fig. 10: T-26 force versus pressure graph.

A. Stepper motor force

The T-26 linear stepper motor has been evaluated using a test bench as shown in Fig. 9. For a range of known masses, the minimum pressure on which the motor could lift the weight was recorded. The results are shown in Fig. 10. The highest measured force was 63 N, at a pressure of 0.65 MPa.

It can be observed that the graph is approximately linear. Its slope is $103\,\mathrm{N/MPa}$. This results in a mechanical efficiency of 43%, when compared with the theoretical force slope of $240\,\mathrm{N/MPa}$.

B. Maximum operating speed

The maximum operating speed (unloaded) was evaluated for all four joints of the Stormram 4 at a pressure of 0.25 MPa, by gradually increasing the stepping frequency until the motor misses steps. The experiment was performed with two different tube lengths, 0.5 m and 5 m. The results are given in Table I. The motor of joint $J4$ appears to have the lowest maximum frequency in both cases.

Under load, the maximum frequency is reduced to approximately 60 Hz for 0.5 m tubes, and 8 Hz for 5 m tubes. At these speeds, the maximum force is maintained for all joints, especially $J4$, as required when inserting the needle into the phantom.

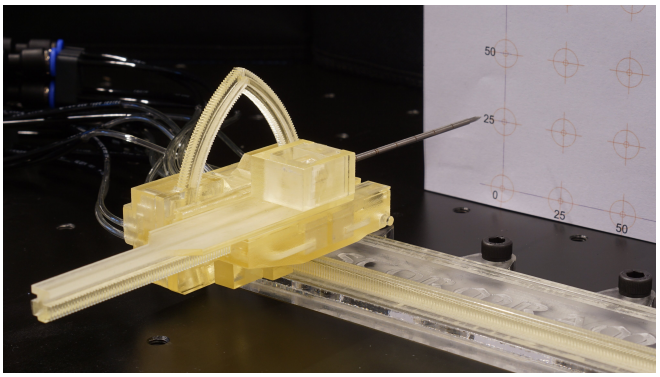

Fig. 11: Accuracy measurement setup.

C. Needle tip accuracy measurements

The positional accuracy was evaluated using a sheet of paper positioned in the Y=80 mm plane, as shown in Fig. 11. On this sheet, a 7x5 grid of targets with 25 mm spacing was drawn. The robot was programmed to move to these targets in succession, resulting in a series of punctures in the sheet. Afterwards, the X and Z offsets of each puncture (relative to its target) were measured.

For every value of Z, the mean target-puncture offsets and the standard deviations were calculated for seven data points, and listed in Table II. It can be observed that at higher Z values, there is an increasing bias in the X direction, resulting in a relative large standard variation of 0.71 mm. But when this systematic offset is taken into account, the standard deviation reduces to 0.20 mm. From the size of the punctures, the accuracy in Y direction is estimated to be 0.2 mm.

A repeatability experiment was performed by executing the same travel path again. For all 35 targets, the needle reached the same spot as in the first run, so no new punctures were created. This can also be observed in the supplementary video. Considering the size of the puncture (average diameter 0.2 mm), the repeatability is therefore better than 0.1 mm.

TABLE I: Maximum unloaded motor stepping frequency.

joint	freq at 0.5 m	freq at 5 m
$J1$	240 Hz	65 Hz
$J2$	240 Hz	50 Hz
$J3$	190 Hz	50 Hz
$J4$	160 Hz	30 Hz

TABLE II: Mean offset μ and standard deviation σ in X and Z directions.

Z [mm]	μ_X [mm]	σ_X [mm]	μ_Z [mm]	σ_Z [mm]
25	-0.49	0.08	-0.04	0.15
50	-0.03	0.09	-0.10	0.16
75	0.40	0.03	0.14	0.08
100	0.96	0.10	0.33	0.13
125	1.46	0.16	0.14	0.18
all	0.46	0.71	0.10	0.21

TABLE III: Comparison of T-26 with T-49. Note: two different housings have been developed for the T-49; the cylindrical one was used in the Stormram 3.

Property	T-26 (Stormram 4)	T-49 (Stormram 3)
Dimensions	26x21x16 mm	⌀56x40 / 49x40x31 mm
Volume	8.7 cm^3	99 cm^3 / 61 cm^3
Force at 0.4 MPa	38 N	96 N
Step size	0.25 mm	1.0 mm
Max freq at 0.5 m	240 Hz (unloaded)	300 Hz (unloaded)
Max freq at 5 m	30 Hz (unloaded), 8 Hz (loaded)	18 Hz (unloaded), 7 Hz (loaded)

V. DISCUSSION

For comparison with the previous version, the properties of the current Stormram 4's T-26 and the T-49 stepper motor of the Stormram 3 are listed in Table III. The T-26 has less than half the strength of the T-49, but the dimension has been reduced approximately a factor two in all directions and the step size is reduced by a factor four.

The maximum frequency was found to be 160-240 Hz when 0.5 m tubes are used. In a MRI setting, 5 m long tubes are required which limits the maximum frequency to 30-60 Hz (unloaded) or 8 Hz (maximum force). Joint $J4$ was found to have the lowest maximum frequencies, presumably due to higher friction and/or air leakage in the motor. The step size is 0.25 mm for the linear motors, so the minimum achievable speed is 2.0 mm/s for 5 m tubes when maximum force is needed. If necessary, this minimum speed could be increased by using a larger step size of 0.5 mm, which doubles the travel speed at the cost of reduced accuracy. A different solution would be to drive a single joint with two motors, to achieve both high speed and high precision.

The positional accuracy of the Stormram 4 is 0.71 mm in X direction, 0.21 mm in Z direction and approximately 0.2 mm in Y direction. This shows that sub-millimeter precision is achieved, which is a significant improvement over the Stormram 3. An important reason is the simplicity of the kinematic design: there are only four joints, and as all of these are directly actuated, the kinematic chain is fully free of backlash.

There is a systematic bias in X direction up to 1.0 mm, likely due to manufacturing inaccuracies. If this bias is compensated for, by e.g. more precise manufacturing and/or calibration, the accuracy can be further improved to 0.17 mm in both X and Z directions. In future iterations of the robot, the structural rigidity could be improved by e.g. duplicating the $J2$ and $J3$ joints to the other side of the robot.

VI. CONCLUSION

The Stormram 4 has demonstrated that it is able to manipulate a needle towards targets with sub-millimeter precision and a measured insertion force of approximately 40 N. The actuators are free of backlash. In a MRI setting, 5 m long tubes are required and the maximum linear movement speed under maximum load is 2.0 mm/s.

The linear and curved motors are significantly smaller with a size of 26 and 30 mm, than the state-of-art motors, and these are efficiently integrated in the different parts of the robot. The novel curved motor has shown that it can actuate a revolute joint with high precision. Due to the serial kinematic chain the number of moving parts are reduced to an absolute minimum, resulting in a design that is compacter than state-of-art robots.

Further tests on breast phantoms in a MRI scanner will be performed to simulate targeting lesions and also take tissue deformations into account. A breast fixation system and a biopsy firing mechanism are improvements to implement the full MRI-guided biopsy procedure in the design. As a proof-of-concept, the Stormram 4 has shown that it is a suitable system to implement in clinical breast biopsy procedures.

ACKNOWLEDGMENTS

The authors would like to thank Gerben te Riet o/g Scholten for 3-D printing the different parts of the Stormram 4.

REFERENCES

[1] J. Ferlay, I. Soerjomataram, M. Ervik, K. Dikshit, S. Eser, C. Mathers, M. Rebelo, D. Parkin, D. Forman, F. Bray. GLOBOCAN 2012 v1.0, Cancer Incidence and Mortality Worldwide: International Agency for Research on Cancer CancerBase; 2012 [Available from: http://globocan.iarc.fr/Pages/fact_sheets_cancer.aspx].

[2] E.R. Price, "Magnetic resonance imaging-guided biopsy of the breast: fundamentals and ner points". Magn Reson Imaging Clin N Am, vol. 21, issue 3, pp. 571581, 2013.

[3] M.C. Chevrier, J. David, M.E. Khoury, L. Lalonde, M. Labelle, I. Trop, "Breast Biopsies Under Magnetic Resonance Imaging Guidance: Challenges of an Essential but Imperfect Technique". Curr Probl Diagn Radiol; vol. 45, issue 3, pp. 193204, 2016.

[4] J. Veltman, C. Boetes, T. Wobbes, J.G. Blickman, J.O. Barentsz, "Magnetic Resonance-Guided Biopsies and Localizations of the Breast: Initial Experiences Using an Open Breast Coil and Compatible Intervention Device". Investigative Radiology, vol. 40, issue 6, pp. 379-384, June 2005.

[5] D. Stoianovici, A. Patriciu, D. Petrisor, D. Mazilu, and L. Kavoussi, "A new type of motor: pneumatic step motor." IEEE/ASME Transactions On Mechatronics, 12(1), 98-106, 2007.

[6] E. Franco, D. Brujic, M. Rea, W. M. Gedroyc and M. Ristic, "Needle-Guiding Robot for Laser Ablation of Liver Tumors Under MRI Guidance," in IEEE/ASME Transactions on Mechatronics, vol. 21, no. 2, pp. 931-944, April 2016.

[7] N. Hungr, I. Bricault, P. Cinquin and C. Fouard, "Design and Validation of a CT- and MRI-Guided Robot for Percutaneous Needle Procedures," in IEEE Transactions on Robotics, vol. 32, no. 4, pp. 973-987, Aug. 2016.

[8] J.G.R. Bomers, D.G.H. Bosboom, G.H. Tigelaar, J. Sabisch, J.J. Ftterer, D. Yakar, "Feasibility of a 2nd generation MR-compatible manipulator for transrectal prostate biopsy guidance", European Radiology, pp. 1-7, July 2016, doi:10.1007/s00330-016-4504-2

[9] V. Groenhuis and S. Stramigioli, "Laser-Cutting Pneumatics," in IEEE/ASME Transactions on Mechatronics, vol. 21, no. 3, pp. 1604-1611, June 2016.

[10] V. Groenhuis, J. Veltman and S. Stramigioli, "Stormram 2: A MRI-compatible pneumatic robotic system for breast biopsy," Proceedings of The Hamlyn Symposium on Medical Robotics, June 2016, Imperial College and the Royal Geographical Society, London, UK, pp. 52-53.

[11] M.E.M.K. Abdelaziz, V. Groenhuis, J. Veltman, F. Siepel and S. Stramigioli, "Controlling the Stormram 2: An MRI-compatible Robotic System for Breast Biopsy". 2017 IEEE International Conference on Robotics and Automation (ICRA), Singapore, 2017, pp. In press.

[12] V. Groenhuis, J. Veltman, F.J. Siepel, S. Stramigioli, "Stormram 3: An MRI-compatible robotic system for breast biopsy" in IEEE Robotics & Automation Magazine, Special Issue on Surgical Robot Challenge, pp. In press.